Article

pubs.acs.org/Biomac

"Docking Sites": Nanometer-Scale Organization of a Reactive, Protein-resistant, Graft Copolymer-Based Interface for Macromolecule Immobilization.

Ning-Ping Huang,*[,†,‡] Susan M. De Paul,[‡,§] and Marcus Textor[‡]

[†]State Key Laboratory of Bioelectronics, School of Biological Science and Medical Engineering, Southeast University, Nanjing, 210096, P.R. China

[‡]Laboratory for Surface Science and Technology, Department of Materials, Swiss Federal Institute of Technology, ETH-Zurich, Wolfgang-Pauli-Strasse 10, 8093 Zurich, Switzerland

Supporting Information

ABSTRACT: The signal-to-noise ratio of a sensor system is determined by the affinity of its active component for the analyte on one hand and its inertness with respect to unrelated stimuli (noise) on the other hand. Nonspecific interactions between the environment and biosensor components (typically constructed from glass, silica, or transition metal oxides) result in nonspecific adsorption onto the latter and constitute a major source of noise. We have previously introduced a polymeric interface for preventing nonspecific adsorption while allowing for high-affinity, specific interactions. It is based on the coassembly of biotinylated and nonbiotinylated poly(L-lysine)-*graft*-poly(ethylene glycol) from aqueous solutions to negatively charged surfaces, such as Nb_2O_5. In this study, we investigated by atomic force microscopy the nanoscale organization of this interface for each individual step involved in the preparation of a bioactive interface: polymer adsorption, loading with streptavidin, and binding of biotinylated vesicles.

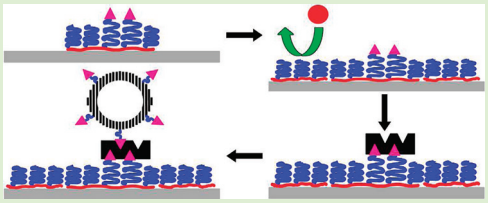

1. INTRODUCTION

Living organisms receive information from their surroundings by means of receptors—molecular devices that are capable of detecting signals from the external environment, including chemical compounds, with very high affinity. Biological sensory systems are also characterized by high selectivity—i.e., the ability to distinguish a given stimulus from a multitude of other, often similar, stimuli that constitute the background noise. The high specificity of biomacromolecules (protein receptors, enzymes, antibodies, etc.), refined by evolution or genetic engineering, makes them ideal candidates for the active ingredients of man-made sensing and processing elements termed biosensors and bioreactors, respectively. The selectivity is engineered into the device by surrounding the sensing element(s) with inert media, much like a cell protects its surface-exposed elements with a polysaccharide coating.[1] The anchoring elements in the resulting island-in-the-sea organization will be referred to as "docking sites" (Figure 1). For such an organization to function efficiently, the interface should be homogeneous, and the density of the docking sites needs to be under strict control.

We have previously demonstrated that coating metal oxide surfaces with a graft copolymer, poly(L-lysine)-*g*-poly(ethylene glycol) (PLL-*g*-PEG),[2,3] protects them from nonspecific adsorption of proteins.[4−7] Furthermore, reactivity has been engineered into this graft copolymer by using reactive poly(ethylene glycol) chains functionalized with, for example, biotin,[6,8,9] an RGD-peptide,[10−13] or the nitrilotriacetic acid (NTA) chelating ligand.[14] In this contribution, we examined the nanoscale organization of this reactive/inert polymeric interface prepared at an oxide surface and followed step-by-step the hierarchical building-up of the biosensor components shown in Figure 1.

2. MATERIALS AND METHODS

All chemicals were sourced from Sigma-Aldrich and used without further purification unless otherwise noted. Ultrapure water (18 MΩ cm^{-1}) obtained from an EasyPure reverse osmosis system (Barnstead Thermolyne, Dubuque, IA) was used both as a solvent and in cleaning processes.

2.1. Buffers. The following two buffers were used in this study: the low ionic strength HEPES-1 (10 mM HEPES, pH 7.4) and the high ionic strength HEPES-2 (10 mM HEPES, 150 mM NaCl, pH 7.4). The buffers were filtered through 0.22 μm Durapore membranes (sterile Millex GV, Sigma-Aldrich) before use.

2.2. Synthesis of PLL-*g*-PEG and Derivatives. A useful nomenclature has been developed to describe the various PLL-*g*-PEG derivatives.[4−6] For example, PLL(20)-*g*[3.5]-PEG(2)/PEGbiotin(3.4)20% denotes a graft copolymer that has a poly(L-lysine) backbone and side chains of poly(ethylene glycol) and biotinylated poly(ethylene glycol). The numbers in parentheses indicate the molecular weights of the reagents, namely, 20 kDa for poly(L-lysine hydrobromide), 2 kDa for SPA- and methoxy-terminated poly(ethylene glycol), and 3.4 kDa for NHS-terminated biotinylated

Received: July 16, 2011
Revised: September 23, 2011
Published: October 31, 2011

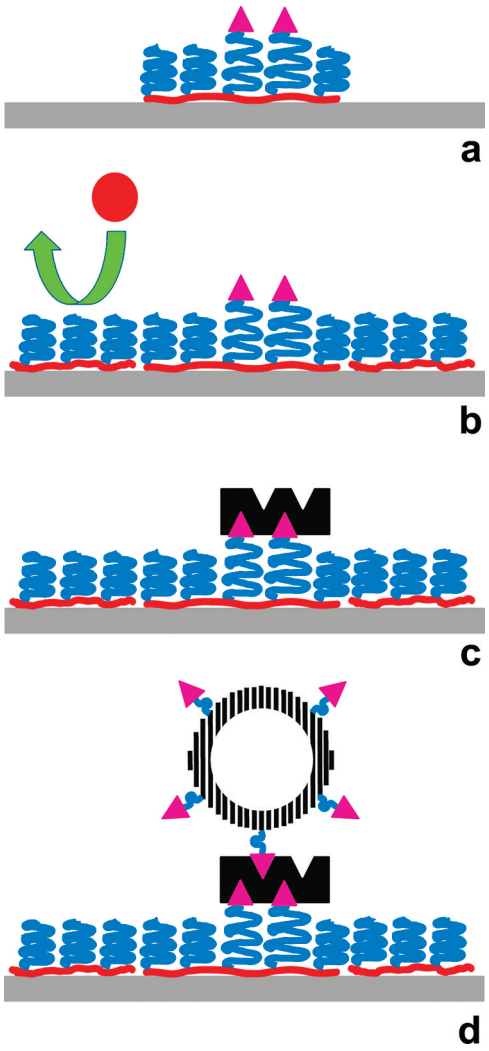

Figure 1. Assembly and molecular organization of the PLL-*g*-PEG – based docking sites architecture. (a) Reactive PLL-*g*-PEG-biotin molecule adsorbed on the surface of a metal oxide. The poly(L-lysine) backbone is shown in red, PEG chains are shown in blue, and reactive sites (biotin molecules in this study), responsible for the specificity of the structure, are depicted as pink triangles. Such organization can be achieved by adsorbing the copolymer from a very dilute solution. (b) Selectivity of the arrangement is ensured by surrounding the reactive site with noninteractive background, composed of nonreactive PLL-*g*-PEG chains. This coating is known to resist nonspecific adsorption of proteins (red ellipsoid). The structure depicted here can be obtained by exposing the bare surface to a mixture of PLL-*g*-PEG and PLL-*g*-PEG-biotin or by adsorbing PLL-*g*-PEG from a pure solution of high concentration to the surface depicted in panel a. Both pathways have been examined in this study. The resulting reactive island, surrounded by the sea of nonreactive material, is referred to as a docking site. (c) Because biotin was used as a model reactive group in this study, the biotinylated surface was further functionalized with streptavidin (black rectangle, with triangular indentations representing the four biotin-binding sites). (d) Streptavidin-bearing docking sites can be used for immobilization of biotinylated species. In this study, biotinylated vesicles were used.

poly(ethylene glycol). The grafting ratio of 3.5 indicates that two out of every seven lysine units are attached to PEG chains, and the designation 20% indicates that one out of five of these PEG chains is biotinylated. For this Article, three types of PLL-*g*-PEG derivatives, PLL(29)-*g*[5.4]-PEG(2), PLL(25)-*g*[3.7]-PEG(2)/PEGbiotin(3.2)-21%, and PLL(357)-*g*[5.4]-PEG(2)/PEGbiotin(3.6)57% were synthesized. Their simplified abbreviations are PLL-*g*-PEG, PPB21, and HMW-PPB57 respectively, and these will be used throughout this Article. Biotin-derivatized PLL-*g*-PEG will also frequently be referred to as PLL-*g*-PEG-biotin.

The PLL-*g*-PEG and PPB21 polymers were synthesized as previously described.[4−6] HMW-PPB57, the biotin-derivatized PLL-*g*-PEG with a high-molecular-weight (HMW) PLL backbone, was synthesized from 357 kDa PLL-HBr, 2 kDa MeO-PEG-SPA, and 3.6 kDa biotin-PEG-CO_2−NHS (both from Nektar, San Carlos, CA) using the same protocol as for PPB21, except that the PLL-HBr solution was not filtered because of its higher viscosity and the corresponding loss of the starting material on the filter membrane. So far, no negative effects have been observed from omitting this sterilization step.

Grafting ratios and percentages of biotinylation were determined by analysis of ^{1}H NMR spectra according to the procedure described in our previous paper.[6] Combining this information with the average reagent molecular weights provided by the manufacturer allowed the total average polymer molecular weights to be calculated, and the results are summarized in Table 1. The adsorption of these three polymers from aqueous solutions onto Nb_2O_5 and the resistance of the resulting polymer layers to nonspecific protein adsorption from human serum were tested by optical waveguide lightmode spectroscopy (OWLS) following the same protocol previously published.[5,6] Within the limits of detection of the OWLS technique (i.e., ∼ 1 ng/cm^2), no human serum was detected on the polymer layer in any of the cases.

2.3. Preparation of Biotinylated Phospholipid Vesicles. Chloroform solutions of dioleoyl phosphatidylcholine (DOPC) and dipalmitoyl phosphatidylethanolamine-lc-biotin (DPPE-lc-biotin) (Avanti Polar Lipids, Alabaster, AL) were mixed in a wt/wt ratio of 9:1. The solvent was evaporated under an argon stream in a fume hood, and the resulting lipidic film was further dried for 30 min in an oven (at room temperature) connected to an oil-free, diaphragm-type vacuum pump. The dry film was suspended in the HEPES-2 buffer at 60 °C to yield multilamellar vesicles (MLVs) at a concentration of 1 mg/mL. Unilamellar vesicles were prepared by extruding a suspension of MLVs through 50 nm pore diameter filters (Avestin, Ottawa, Canada) ∼30 times using a Lipofast extruder (Avestin).[15,16] The extruder and the vesicle solution were kept above 60 °C during this step. Vesicle solutions were stored under argon at 4 °C for a maximum of 2 weeks before use.

2.4. Substrate Preparation and Cleaning. Silicon wafers (1 × 1 cm^2, Powatech, Cham, Switzerland) were sonicated twice in toluene for a total of 30 min to remove organic contamination prior to coating. A 20 nm thick layer of Nb_2O_5 was sputter-coated on the clean silicon wafers in a Leybold dc-magnetron Z600 sputtering unit by using reactive magnetron sputtering (PSI, Villigen, Switzerland).[17]

Immediately before use, the 1 × 1 cm^2 pieces of Nb_2O_5-coated silicon wafer were sonicated in 2-propanol for 10 min and in ultrapure water for another 10 min, dried in a stream of nitrogen, and cleaned for 2 min in oxygen plasma in a Plasma Cleaner/Sterilizer PDC-32G (Harrick, Ossining, NY). The clean Nb_2O_5 substrates were glued onto steel discs covered with PTFE-adhesive tape (BYATC, Norton Performance Plastics Corporation, Akron, OH) according to the procedure of Mueller et al.[18] using double-sided tape.

2.5. Surface Modification. We deposited 20 μL of a solution of a given polymer at a specified concentration in the selected buffer onto a clean Nb_2O_5 sample (prepared as described above) and incubated for 15 min at room temperature. The surface was then rinsed with the same buffer to remove the unattached molecules. The choice of polymer and its concentration depended on the goal of the experiment, and the various protocols are summarized in Table 2. The conditions for attachment of streptavidin and decoration of the resulting docking sites with the vesicles can also be found in Table 2.

2.6. Atomic Force Microscopy. AFM images were collected in an appropriate buffer (indicated in the figure captions) in contact mode with a Nanoscope IIIa Multimode AFM (Veeco, Santa Barbara, CA) equipped with a "J" (120 μm) scanner, using oxide-sharpened silicon nitride tips mounted on V-shaped 200 μm long silicon nitride cantilevers with a nominal spring constant of 0.06 N/m (NP-S,

Table 1. Characteristics of the Polymers Used in This Study

polymer abbreviation	polymer nomenclature[a]	grafting ratio	% of PEG chains biotinylated[b]	average molecular weight (kDa)
PLL-*g*-PEG	PLL(29)-*g*[5.4]-PEG(2)	5.4 ± 0.5	0	68
PPB21	PLL(25)-*g*[3.7]-PEG(2)/PEGbiotin(3.2)21%	3.7 ± 0.5	21 ± 5	83
HMW- PPB57	PLL(357)-*g*[5.4]-PEG(2)/PEGbiotin(3.6)57%	5.4 ± 0.5	57 ± 5	1096

[a]In the established PLL-*g*-PEG nomenclature,[4−7] the molecular weights of the reagents are listed in parentheses, but the calculated average molecular weights took into account the departure of the leaving groups (e.g, NHS) as well as the removal of the bromine from the PLL-HBr by dialysis. [b]Estimated error is due to partial peak overlap and imperfect baselines in ^{1}H NMR spectra.

Table 2. Polymer Adsorption, Streptavidin Loading, and Vesicle Decoration Protocols Used in the Various Experiments

experiment[a]	reagent[b]	concentration[c]
visualizing single polymer molecules	PPB21, HMW-PPB57[d]	1.5 nM
polymer adsorption	PPB21	1.5 nM, 3.75 nM, 7.5 nM, 15 μM
one-step adsorption (prior to streptavidin binding and vesicle decoration)	PPB21 + PLL-*g*-PEG, various ratios	15 μM
streptavidin binding[e]	streptavidin	0.1 mg/mL
vesicle decoration[e]	DOPC: DPPE-lc-biotin, 9:1	50 μg/mL

[a]All polymer adsorption steps were done in HEPES-1 buffer unless stated otherwise. Streptavidin and vesicles were adsorbed from HEPES-2 buffer. All AFM images were taken in HEPES-2 buffer unless stated otherwise. [b]Adsorption times were 15 min for each steps. [c]20 μL of solution was added. [d]In some experiments, the adsorption step was repeated two or three times. [e]Before addition of streptavidin and vesicles, the surface was washed with HEPES-2 buffer.

Veeco). The fluid cell was washed extensively with a 2% sodium dodecyl sulfate solution and rinsed with ultrapure water before each experiment. An O-ring was not used. Sample exchange was carried out ex situ to prevent adsorption of polymers and proteins onto the surface of the AFM tip. The microscope was allowed to equilibrate for a minimum of 30 min before imaging. Trace and retrace images were collected and compared. Images were flattened and plane-fitted as required.

3. RESULTS AND DISCUSSION

Typically, a biosensor, such as one shown in Figure 1d, is built up in a hierarchical fashion. In this particular case, the polymer surface was built up first, either by adsorbing the reactive (in this case, biotinylated) polymer from a dilute solution (Figure 1a) and then backfilling the remaining available surface space with an inert (nonbiotinylated) polymer or by adsorbing reactive and inert polymers together from a mixed solution. In both cases, a surface of reactive sites surrounded by an inert matrix was obtained (Figure 1b). Because biotin was the biointeractive molecule in this study, the reactive polymer was subsequently modified by adding streptavidin (Figure 1c). (Related proteins such as avidin and NeutrAvidin could also have been used, as was shown previously.[6]) In the final step, the streptavidin-bearing docking sites could be functionalized with the biotinylated reagent of choice, such as an antibody,[6,19] peptide,[20] enzyme,[8] or a reactive "container".[21−23] Biotinylated vesicles were chosen in this study to serve as a well-defined model system (Figure 1d).

In view of this hierarchical organization, this section is subdivided into three subsections corresponding to these three assembly steps.

3.1. Organization of PLL-*g*-PEG/PLL-*g*-PEG-biotin Mixtures on Oxide Surfaces. *3.1.1. Visualizing Individual Biotin-Derivatized PLL-g-PEG Molecules.* The driving force for the adsorption of PLL-*g*-PEG derivatives onto an oxide surface is the electrostatic interaction between the positively charged poly(L-lysine) backbone and the negatively charged oxide surface.[4,5,24,25] Therefore, the copolymer is best adsorbed from a low ionic strength buffer (HEPES-1). Low ionic strength not only increases the long-range electrostatic interaction but also influences the conformation of the polycationic polymer (i.e., the backbone is more stretched out), both of which lead to a flat and dense organization of the polymer at the interface. The topography of a PLL-*g*-PEG/PEGbiotin submonolayer was imaged by AFM in two buffer solutions (Figure 2). Figure 2a indicates that the copolymer is

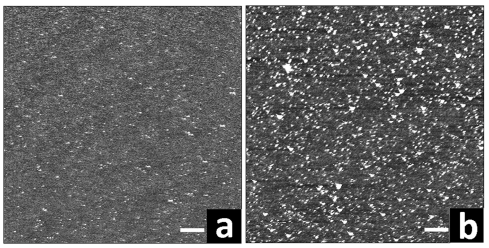

Figure 2. Effect of ionic strength on AFM imaging of a PLL-*g*-PEG-biotin polymeric layer prepared by incubating a Nb_2O_5 substrate with a 2.5 nM solution of PPB21 in HEPES-1 buffer (10 mM HEPES, pH 7.4). (a) Image of the polymeric layer in HEPES-1 buffer. (b) The sample shown in panel a, after washing with and imaging in HEPES-2 buffer (10 mM HEPES, 150 mM NaCl, pH 7.4). Scale bar: 250 nm, *Z*-scale: 5 nm.

essentially invisible to AFM in HEPES-1 due to the electrostatic repulsion between the negatively charged tip and the negatively charged surface of the oxide.[26] It has been demonstrated that electrostatic interactions between the AFM tip and the sample[24,25,27] can influence the measured height of a biological structure adsorbed to a solid support in a buffer solution.[26] To lessen these repulsive interactions, the surface of Figure 2a was subsequently washed with and then immersed in a higher ionic strength buffer (HEPES-2, containing 150 mM NaCl). The resulting image (Figure 2b) confirms that the repulsive electrostatic interactions were largely screened, leading to an enhancement of the image contrast and to visualization of the copolymer. The effect of the ionic strength on the interaction between the negatively charged AFM tip and the bare Nb_2O_5 surface and on the interaction between the AFM tip and the PLL-*g*-PEG-coated Nb_2O_5 surface has been previously investigated.[28] Previous studies have also shown that exposure of surface-adsorbed PLL-*g*-PEG to physiological ionic strength

solution does not alter the adsorbed mass and protein resistance of the coating.[4] Therefore, HEPES-2 buffer was taken as the imaging buffer for all AFM experiments carried out in this Article, although the polymer deposition step was always carried out using HEPES-1.

To visualize individual polymer molecules and determine the size of a single molecule, we imaged Nb_2O_5 substrates exposed to polymer solutions at low enough concentrations to achieve submonolayer coverage. Figure 3 shows the topographic image

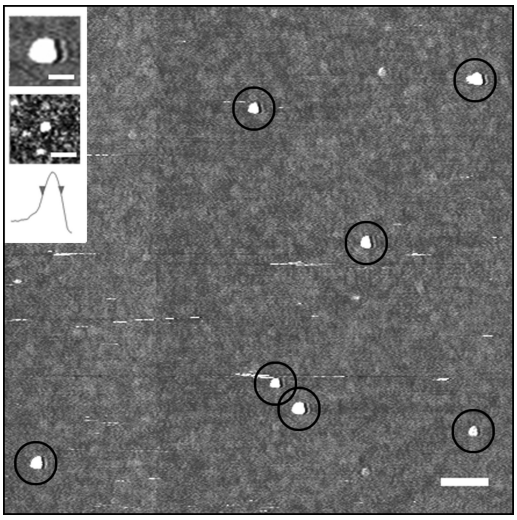

Figure 3. Visualizing individual PLL-*g*-PEG-biotin molecules. Nb_2O_5 substrate incubated with 20 μL of 1.5 nM solution of HMW-PPB57 in HEPES-1 buffer for 15 min, washed, and imaged in HEPES-2 buffer. White circular objects (encircled in black) are single polymer molecules. Top inset: a view of one of the encircled molecules. Middle inset: a view of a molecule of 87 kDa PPB21 imaged under identical conditions. Scale bars: 200 nm, 50 nm (insets). *Z*-scale: 3 nm. Average diameters, calculated as full widths at half-height (bottom inset), were 19 ± 6 nm (171 measurements) for the 83 kDa polymer and 34 ± 7 nm (167 measurements) for the 1096 kDa polymer.

of a submonolayer formed from high-molecular-weight PLL-*g*-PEG/PEGbiotin (~1096 kDa, HMW-PPB57) (see Figure S1 of the Supporting Information for the corresponding 3D image) and two typical single polymer molecules (insets) with different molecular weights. It was possible to use AFM to distinguish between copolymers of two different molecular weights, ~ 83 and ~1096 kDa (Table 1). The absolute values of molecular diameters, as measured by AFM, were 19 ± 6 nm (171 measurements) for the 83 kDa polymer (PPB21) and 34 ± 7 nm (167 measurements) for the 1096 kDa polymer (HMW-PPB57)

A rough approximation of the size of the PLL-*g*-PEG-biotin molecule can be obtained from a spherical model, assuming that the PLL backbone is randomly coiled with loops and tails on the surface. Although this model does not necessarily reflect the true conformation of surface-bound PLL-*g*-PEG, it permits an estimation of the approximate sizes of the two molecules. The volume of the PLL-*g*-PEG-biotin molecule is then taken as the sum of volumes occupied by the PEG and PEGbiotin chains. The radius of gyration (R_g) of PEG or PEGbiotin chains can be estimated using an empirical equation based on static light scattering measurements,[29] $R_g = 0.181(N)^{0.58}$ (nm), where N is the number of repeat units for the PEG. The number of PEG or PEGbiotin chains is calculated from the grafting ratio and the biotinylation percentage. Assuming that the PLL-*g*-PEG-biotin molecule is a sphere permits an estimation of the volume and thus the diameter from the sum of the volumes of the PEG chains. (See Table S2 of the Supporting Information for the details of the calculation.) The expected diameters were found to be ~11 nm for the 83 kDa polymer and ~27 nm for the 1096 kDa one.

Of course, one would not expect the PLL-*g*-PEG molecules to be perfectly spherical when adsorbed on a metal oxide surface. Electrostatic attractions would likely pull the poly(L-lysine) backbone closer to the surface, leading to flattening of the spheres and to a corresponding increase in the effective radius of the area occupied by the polymer on the surface. In addition, the effects of tip convolution, electrostatic interactions between the AFM tip and the sample, and the error bars on the grafting ratio and the biotinylation percentage would also be expected to play a role. Nonetheless, the size values of both types of PPB obtained from the AFM images are close enough to those obtained from the spherical model to permit us to conclude that the objects visible in Figure 3 are individual polymer molecules.

3.1.2. Assembly of the PLL-g-PEG/PLL-g-PEG-biotin Layer: Sequential versus One-Step Adsorption of Reactive and Inert Polymers. The ability to visualize individual polymer molecules makes it possible to follow the process of PLL-*g*-PEG-biotin adsorption onto the oxide surface. For that purpose, a dilute solution of polymer (Table 2) was allowed to adsorb to the surface, which was subsequently imaged. This procedure was repeated a number of times using different concentrations and, in some cases, sequential exposure to two or more concentrations, creating a series of images of increasingly dense polymer coverage such as the one shown in Figure 4. (See Figure S1 of the Supporting Information for the corresponding 3D images of adsorption of polymer.)

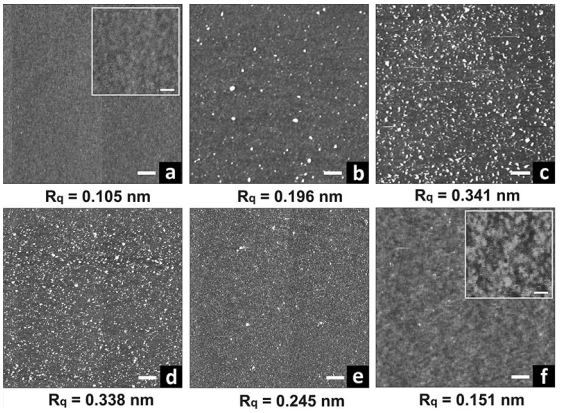

Figure 4. AFM images of adsorption of PLL-*g*-PEG-biotin (PPB21) on Nb_2O_5 substrates produced by 15 min of incubation with 20 μL of PPB21 at different concentrations in HEPES-1 buffer solutions. (a) 0 nM ; (b) 1.5 nM; (c) 3.75 nM; (d) 7.5 nM; (e) 7.5 nM PPB21 was again injected onto the surface shown in (d); (f) 15 μM PPB21 was injected onto the surface shown in (e). The imaging was performed in HEPES-2 buffer. Scale bars: 250 nm, 100 nm (insets). *Z*-scale: 5 nm, 3 nm (insets). The value of R_q (root-mean-square roughness) corresponding to each image is given.

Figure 4a shows the bare Nb_2O_5 substrate imaged in HEPES-2 buffer. It is flat and featureless with a root-mean-square roughness (R_q, the root-mean-square of the values of all points of the profile) of 0.105 nm over an area of 6.25 μm^2. Upon the

injection of 20 μL of 1.5, 3.75, or 7.5 nM PLL-*g*-PEG-biotin (e.g., PPB21) solution, the substrates were partially covered with the PPB21 molecules, as shown in Figure 4b–d, respectively. At low surface coverage (Figure 4b), the polymer molecules are seen to be well-separated from each other and are randomly distributed over the surface with no evidence of significant clustering. The surface density of the molecules is seen to increase approximately uniformly with the amount of the polymer added to the surface (Figure 4b–d). When another 20 μL of 7.5 nM PPB21 was added to the submonolayer that was previously produced by the injection of 7.5 nM PPB21 solution (corresponding to Figure 4d), the surface coverage of adsorbate increased again, and the surface became smoother (Figure 4e). The resulting surface was then backfilled with 15 μM PPB21 to achieve a full PLL-*g*-PEG-biotin monolayer (Figure 4f) with a root-mean-square roughness of 0.151 nm over an area of 6.25 μm^2.

Because the adsorption of PLL-*g*-PEG and its derivatives onto a Nb_2O_5 substrate is driven by electrostatic interactions between the positively charged PLL backbone and the negatively charged substrate, the surface coverage of PPB21 can be easily increased by introducing more adsorbates either through an increase in the PPB21 concentration or through the repeated addition of PPB21 solution as long as the substrate is not fully covered. According to the R_q values corresponding to each image (Figure 4), as the surface coverage of PPB21 increased from 0 to 100%, the surface initially became rougher until reaching a maximum. Then, it started becoming smoother as more of the substrate was covered by PPB21, until a full PPB21 monolayer was ultimately formed. The roughness of the PPB21 monolayer formed by sequential adsorption (R_q = 0.151 nm) is found to be close to or only slightly larger than that of monolayer formed in one step by quickly exposing the bare surface to a high concentration (15 μM) of PPB21 (R_q = 0.137 nm). We suppose that during the sequential adsorption of PPB21, polymer molecules essentially stick to whatever part of the substrate with which they first come in contact and that they are randomly distributed. Additionally, the mixed polymeric surfaces (e.g., PPB21-5%, PPB21-10%, or PPB21-50%) produced from a single deposition of a high-concentration polymer mixture (5% of PPB21 and 95% PLL-*g*-PEG, 10% of PPB21 and 90% PLL-*g*-PEG, or 50% of PPB21 and 50% PLL-*g*-PEG) were still relatively smooth and homogeneous (Figure 5a–c, with R_q values of 0.150, 0.160, 0.170 nm, respectively) although two different species containing different lengths of grafted chains (~2 kDa for PEG and ~3.2 kDa for PEGbiotin) exist on the surface. The likely reasons are that the two polymers were well mixed before being introduced onto the surface and that both polymers are flexible.

3.2. Binding of Streptavidin to the PLL-*g*-PEG/PLL-*g*-PEG-biotin Layers. As we have previously shown,[6] pure PLL-*g*-PEG surfaces with an appropriate grafting ratio are resistant (to <1 ng/cm^2) to the adsorption of many proteins including streptavidin, but inclusion of biotinylated PEG chains in the interface permits the selective capture of streptavidin molecules by the biotin moieties.

The addition of streptavidin markedly changed the morphology of the mixed PLL-*g*-PEG/PLL-*g*-PEG-biotin interfaces. After 15 min of incubation and a rinse with HEPES-2 buffer, the homogeneous films (saturated monolayer) that were obtained after the one-step adsorption of the polymers from a mixture (Figure 5a–c) were converted to

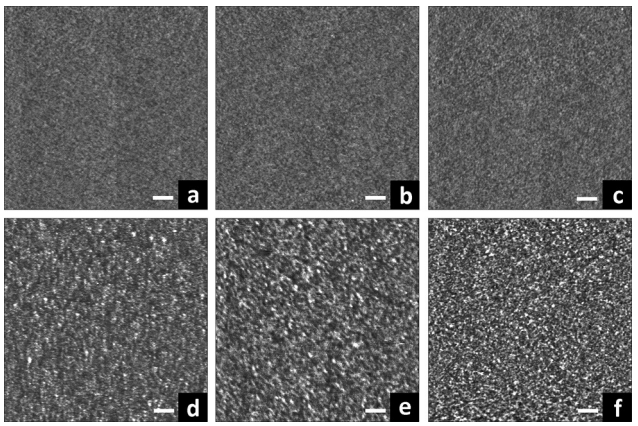

Figure 5. Mixed polymeric interfaces of biotinylated and non-biotinylated PLL-*g*-PEGs prepared by one-step adsorption from 15 μM solution containing different ratios of PPB21 and PLL-*g*-PEG: (a) PPB21-5%, (b) PPB21-10%, (c) PPB21-50%, and the morphology after loading with streptavidin on (d) PPB21-5%, (e) PPB21-10%, and (f) PPB21-50%. Scale bar: 250 nm. *Z*-scale: 5 nm.

rougher surfaces exhibiting patterns of bright spots (Figure 5d–f). Qualitatively, the density of these spots correlated with the concentration of the PLL-*g*-PEG-biotin in the mixture used to prepare the interface (Figure 5d–f). Previous work from our group shows that the ratio of the two polymers in solution determines their ratio on the surface,[6] and thus the density of the white spots correlates with the surface density of the biotinylated copolymer.

In ~45% of the images (i.e., 5 out of 11 experiments), the white spots were organized in clear stripe-like patterns (Figure

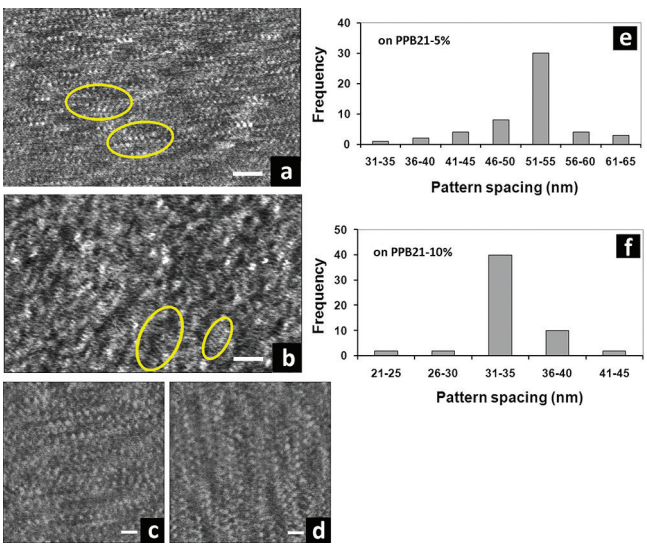

Figure 6. Morphology of streptavidin-loaded PLL-*g*-PEG/PLL-*g*-PEG-biotin layers and distributions of spacing in streptavidin-induced patterns on two different mixed polymeric interfaces (a,e: PPB21-5% and b,f: PPB21-10%). For easier recognition, typical stripe-like patterns are marked by frames (a and b). The same area of streptavidin-loaded PPB21-5% surface was imaged at scan angles of 90 (c) and 0° (d), respectively. Scale bars: 250 (a,b) and 100 nm (c,d). *Z*-scale: 5 nm.

6a,b). This phenomenon was never observed on mixed polymeric interfaces alone but only after the addition of streptavidin. Pattern orientation was found to change when the

dx.doi.org/10.1021/bm2009872|*Biomacromolecules* 2011, 12, 4213–4220

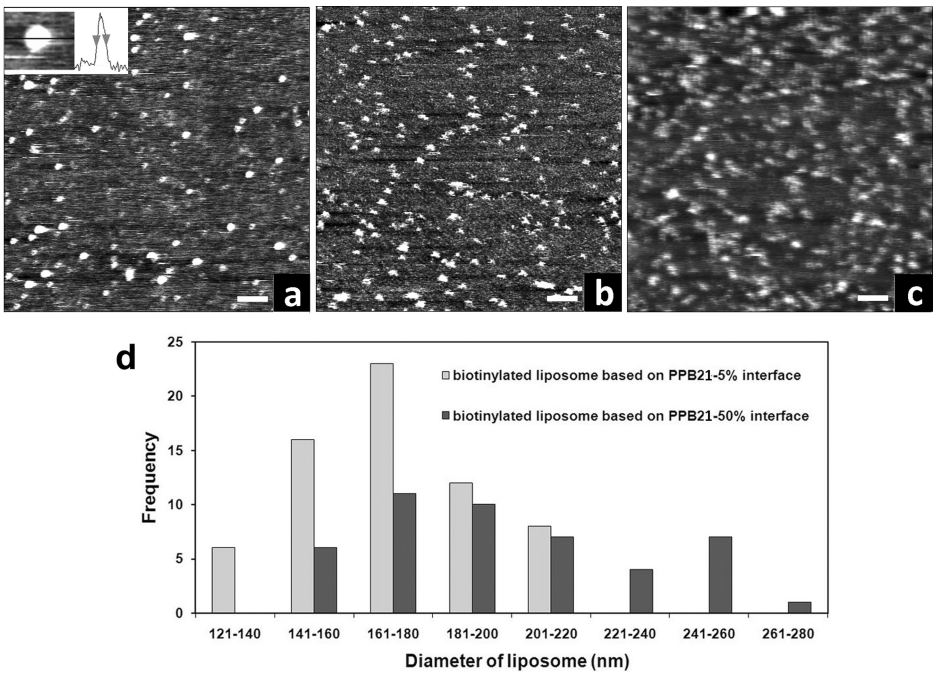

Figure 7. Biotinylated liposomes bound to a streptavidin layer that in turn is bound to a polymeric interface of (a) PPB21-5%, (b) PPB21-10%, and (c) PPB21-50%. Scale bar: 1 μm. *Z*-scale: 5 nm for (a,b) and 30 nm for (c). Inset of panel a: The diameter of a liposome was measured between the two markers. (d) Distributions of liposome size based on two different mixed polymeric interface (PPB21-5% and PPB21-50%).

scan angle was changed (Figure 6c,d), indicating that the features are not simply due to tip artifacts. Pattern spacing (e.g., the distance between the centers of the two adjacent white spots) determined from the image of PPB21-5% (i.e., mixed polymer layers containing 5% of PPB21) was 52 ± 6 nm (Figure 6a,e), and that from the image of PPB21-10% (i.e., mixed polymer layers containing 10% of PPB21) was 34 ± 4 nm (Figure 6b,f). The average distances between the two different neighboring PPB21 molecules in the two cases, estimated from the adsorbed polymer mass measured by OWLS,[6] were approximately 37 and 26 nm, respectively. (See Table S3 of the Supporting Information for the details of the calculation.) We presume that the pattern spacing determined from AFM corresponds to the distance between biotinylated PLL-*g*-PEG molecules (PPB21) embedded in the matrix of nonbiotinylated PLL-*g*-PEG. As shown in previous OWLS experiments,[6] one molecule of PPB21 captures an average of one molecule of streptavidin, despite the presence of ~6.7 biotin molecules per polymer chain. A combination of inaccessible biotinylated chains, steric hindrance, and the binding of more than one biotinylated PEG group to a single streptavidin likely explains the apparent discrepancy between the number of biotin moieties on the surface and the number of bound streptavidin molecules. The discrepancy between the OWLS and the AFM results may be partially due to the error bars on the grafting ratio and the biotinylation percentage and a simple model for estimation.

The origin of the change in the surface morphology that is observed upon binding of streptavidin to the copolymer lies in the difference in mechanical properties between the copolymer (soft)[28] and streptavidin (stiff).[30] When streptavidin is added, it binds to the PPB21 molecules only, making them stiffer and higher than their surrounding nonbiotinylated PLL-*g*-PEG molecules. Why in some instances a pattern of stripes is observed whereas in other instances the white spots have a random, isotropic orientation remains unclear.

3.3. Vesicle Immobilization on PLL-*g*-PEG/PLL-*g*-PEG-biotin:Streptavidin Layers. Loading the streptavidin-bearing reactive sites with an effector entity normally completes the biosensor assembly process. Examples of suitable effectors include biotinylated antibodies,[6] biotinylated nucleic acids,[31] and biotinylated enzymes.[8] Our group has previously demonstrated the specificity of the addition of a biotinylated antibody effector to streptavidin-coated PLL-*g*-PEG/PLL-*g*-PEG-biotin layers.[6] In that study, control experiments verified that whereas the streptavidin molecules on a PLL-*g*-PEG/PLL-*g*-PEG-biotin layer could successfully capture biotinylated α-RIgG molecules, the streptavidin-coated PLL-*g*-PEG/PLL-*g*-PEG-biotin-functionalized surface is strongly resistant to both adsorption of nonbiotinylated RIgG molecules and adsorption of proteins from serum. These results reveal the promise of the docking site approach for effective capture and immobilization of biotinylated effector molecules.

In recent years, a strong interest in containerized effectors has developed. Suitable containers include lipidic or polymeric vesicles, which offer protection to the effector molecule, amplify the response signal in a cascade, and possibly further increase the signal-to-noise ratio by preventing nonspecific interactions.[22,32−37] An additional advantage of using lipidic or polymeric vesicles in the AFM experiments is their visibility.[16,38−42] We, therefore, chose biotinylated lipidic vesicles as markers of streptavidin-bearing sites, in an effort to characterize further the morphology of the PLL-*g*-PEG/PLL-*g*-PEG-biotin interface as well as to demonstrate the suitability of this interface for anchoring the lipidic containers as an alternative to less efficient blocking and anchoring systems.[43]

Biotinylated vesicles of ~50 nm in diameter were added to streptavidin-modified PLL-*g*-PEG/PLL-*g*-PEG-biotin interfaces containing 5, 10, and 50% of the biotinylated copolymer PPB21

~1 h after assembly of the streptavidin layer (due to the time required for AFM equilibration and imaging of the streptavidin-coated polymer). After 15 min of incubation and a rinse with HEPES-2 buffer, vesicles are clearly visible in the AFM images (Figure 7a–c). They are distributed randomly and appear well-separated on samples with 5 and 10% of PPB21 (Figure 7a,b) but are more densely packed on the PPB21-50% surfaces. Individual vesicles can clearly be discerned in the images of the samples with low coverage. (See the inset in Figure 7a.) Qualitatively, the density of the vesicles increased with the amount of PPB21 present in the copolymer mixture. This confirms that molecules of biotinylated PLL-*g*-PEG are homogeneously distributed within the matrix of nonbiotinylated PLL-*g*-PEG even when deposition occurs simultaneously from a mixture of the two polymers.

However, the vesicle coverage is very sparse compared with the streptavidin density determined from the AFM measurements described in Section 3.2: the observed spacing between neighboring PPB21 molecules (and, therefore, between neighboring streptavidin molecules) is ~52 nm for the PPB21-5% layer, which means that the area surrounding each docking site that would be available to the effector molecule is ~2700 nm^2, which is slightly larger than that occupied by a 50 nm vesicle (~2000 nm^2). Clearly, only a small fraction of the streptavidin sites are being functionalized by the vesicles (Figure 7a).

The observation that the number of effector molecules bound to the reactive sites is smaller than that expected from the number of sites available has been reported for other polymer brush-based systems.[44] At least two possible causes can be suggested. First, it is well-known that the ends of the individual chains within the brush are distributed around a distance 0.7*L* from the surface, where *L* is the thickness of the brush.[45] Therefore, at any given time, only a fraction of all of the reactive streptavidin groups will be available. As shown in previous OWLS experiments,[6] approximately one molecule of biotinylated α-RIgG is captured for every three to four molecules of streptavidin, and approximately one molecule of biotinylated bovine serum albumin is captured for every two to three molecules of streptavidin based on the mixed polymer layers containing 0–60% of PPB21. Second, the flexibility of the biotinylated PEG chains could allow the streptavidin to be tilted at some angle with respect to the surface, permitting more than two of the PEG-biotins to bind to a single streptavidin molecule, thus reducing the number of active sites of streptavidin available for further binding to the vesicles. This process is time-dependent, and we have indeed observed that maximum coverage is only achieved if the samples are incubated with biotinylated effector molecules immediately after the preparation of the streptavidin-loaded polymer interface.[6] In the present experiments, biotinylated vesicles were added ~1 h after the preparation of the streptavidin-modified sample (which was performed by incubating the polymer sample with streptavidin in HEPES-2 for 15 min and washing with HEPES-2) because of the time needed for manipulation and equilibration of the AFM instrument and scanning of the streptavidin layer. Therefore, a slower reconstruction process presumably occurred, during which additional PEGbiotin groups could bind to the streptavidin, thus reducing the average number of free sites available for subsequent binding to the biotinylated vesicles. If the kinetics of adsorption of the biotinylated vesicles were also slower than for molecules such as biotinylated α-RIgG and biotinylated bovine serum albumin, this would make the vesicle coverage even sparser.

Histograms of the vesicle size distributions on streptavidin-coated PPB21-5% and PPB21-50% interfaces are shown in Figure 7d. By comparing the histograms, we concluded that the vesicles on PPB21-5% (Figure 7a) exist primarily as isolated spheres with a mode diameter of 161–180 nm, whereas the PPB21-50% surface shows a combination of both single vesicles and aggregated clusters. This aggregation might be attributed to the high surface biotin concentration and thus the high amount of adsorbed streptavidin. A fraction of further captured vesicles might be too close to be resolved into individual vesicles. In stark contrast with the previously reported observations on mica,[16,39] the diameter of the individual vesicles bound to the copolymer measured in the AFM images (Figure 7d) was much larger than expected (~50 nm). We believe this to be the result of a tip convolution artifact. Several effects conspire to make the effect of tip convolution much more pronounced in the case of the vesicles bound to the copolymer layer than in the case of vesicles immobilized on the surface of mica. First, vesicles adsorbed on mica are deformed due to the interaction between the surface and the lipids.[46] Deformation decreases the height of the adsorbed vesicles. Vesicles bound to the copolymer interface are not deformed. Second, electrostatic repulsion between the tip and the surface of mica further diminishes the effective height of the vesicles.[26] In contrast with this, the tip is likely to penetrate into the copolymer layer or compress the copolymer layer to some degree. Therefore, whereas the effect of the electrostatic repulsion and vesicle deformation on mica is to decrease the tip-vesicle interaction area and therefore reduce the magnitude of tip convolution, on the PLL-*g*-PEG-covered surface, it is the opposite.

4. CONCLUSIONS

Atomic force microscopy was used to investigate the lateral organization of the polymer mixture of PLL-*g*-PEG and PLL-*g*-PEG-biotin on a Nb_2O_5 support. By choosing a buffer solution of a suitable ionic strength, electrostatic forces between the AFM tip and the sample were reduced, and the diameter of individual polymer molecules could be successfully measured at submonolayer coverage. During the formation of a PLL-*g*-PEG-biotin monolayer from its submonolayer, no phase segregation (no island formation) was observed. The mixed polymeric interface of PLL-*g*-PEG and PLL-*g*-PEG-biotin, produced by simultaneous adsorption and leading to full monolayer coverage, was investigated by labeling the biotinylated polymers with streptavidin and subsequently exposing the interface to large unilamellar biotinylated liposomes. Consequently, the location of some of the biotin sites on PLL-*g*-PEG-biotin molecules was made visible to the AFM tip. The distribution of the biotinylated polymers within the noninteractive PLL-*g*-PEG matrix, reflected by the distribution of liposomes, was found to be random and homogeneous and to increase as a function of the PLL-g-PEG-biotin concentration. This is an important finding because it provides a rational for the excellent response found with mixed PLL-*g*-PEG/PLL-*g*-PEG-X monolayers, including the often observed linear response with increasing fraction of the functionalized copolymer, both of which would not be expected if substantial phase separation would occur. We propose that the architecture of the mixed adlayers reflects an adsorption regime where the copolymer molecules once adsorbed to the surface, are either trapped or able to diffuse over only very small (nanometer) dimensions. It is also likely

that this is a general property of the PLL-*g*-PEG/PLL-*g*-PEG-X system forming a monolayer with multiple electrostatic adhesions to the surface, and not dependent on the nature of the functionality X. This is furthermore relevant in the light of the wide and successful use of functionalized PLL-*g*-PEG compounds, with, apart from biotin, functionalities such as peptides, carbohydrates, and NTA, some of which are available commercially.

■ ASSOCIATED CONTENT

Supporting Information

3D AFM images of adsorption of PLL-*g*-PEG-biotin on Nb_2O_5 substrates, estimation of the size of the PLL-*g*-PEG-biotin molecule, estimation of the distance between neighboring PPB21 molecules on the surface of PPB21-5% and PPB21-10% from the adsorbed polymer mass measured by OWLS. This material is available free of charge via the Internet at http://pubs.acs.org.

■ AUTHOR INFORMATION

Corresponding Author

*E-mail: nphuang@seu.edu.cn. Tel.: +86 25 8379 0820. Fax: +86 25 8379 5635.

Present Address

[§]Solvias AG, Römerpark 2, CH-4303 Kaiseraugst, Switzerland.

■ ACKNOWLEDGMENTS

We thank Ilya Reviakine (CIC bioMAGUNE, Spain) for support with the initial AFM experiments as well as for many valuable and insightful discussions. Financial contributions from the Swiss National Science Foundation (SNF, National Research Program NFP 47 "Supramolecular Functional Materials") and from the Swiss Federal Commission for Technology and Innovation (CTI, project no. 4620.1 MTS) are gratefully acknowledged. N.-P. Huang acknowledges the financial support from the National Science Foundation of China (no. 30870626).

■ REFERENCES

(1) Englund, P. T. *Annu. Rev. Biochem.* **1993**, *62*, 121−138.
(2) Sawhney, A. S.; Hubbell, J. A. *Biomaterials* **1992**, *13*, 863−870.
(3) Elbert, D. L.; Hubbell, J. A. *Chem. Biol.* **1998**, *5*, 177−183.
(4) Kenausis, G. L.; Voros, J.; Elbert, D. L.; Huang, N. P.; Hofer, R.; Ruiz-Taylor, L.; Textor, M.; Hubbell, J. A.; Spencer, N. D. *J. Phys. Chem. B* **2000**, *104*, 3298−3309.
(5) Huang, N. P.; Michel, R.; Voros, J.; Textor, M.; Hofer, R.; Rossi, A.; Elbert, D. L.; Hubbell, J. A.; Spencer, N. D. *Langmuir* **2001**, *17*, 489−498.
(6) Huang, N. P.; Voros, J.; De Paul, S. M.; Textor, M.; Spencer, N. D. *Langmuir* **2002**, *18*, 220−230.
(7) Pasche, S.; De Paul, S. M.; Voros, J.; Spencer, N. D.; Textor, M. *Langmuir* **2003**, *19*, 9216−9225.
(8) Zhen, G. L.; Eggli, V.; Voros, J.; Zammaretti, P.; Textor, M.; Glockshuber, R.; Kuennemann, E. *Langmuir* **2004**, *20*, 10464−10473.
(9) Raichur, A. M.; Voros, J.; Textor, M.; Fery, A. *Biomacromolecules* **2006**, *7*, 2331−2336.
(10) VandeVondele, S.; Voros, J.; Hubbell, J. A. *Biotechnol. Bioeng.* **2003**, *82*, 784−790.
(11) Tosatti, S.; Schwartz, Z.; Campbell, C.; Cochran, D. L.; VandeVondele, S.; Hubbell, J. A.; Denzer, A.; Simpson, J.; Wieland, M.; Lohmann, C. H.; Textor, M.; Boyan, B. D. *J. Biomed. Mater. Res., Part A* **2004**, *68A*, 458−472.
(12) Schuler, M.; Owen, G. R.; Hamilton, D. W.; De Wilde, M.; Textor, M.; Brunette, D. M.; Tosatti, S. G. P. *Biomaterials* **2006**, *27*, 4003−4015.
(13) Vonwil, D.; Schuler, M.; Barbero, A.; Strobel, S.; Wendt, D.; Textor, M.; Aebi, U.; Martin, I. *Eur. Cells Mater.* **2010**, *20*, 316−328.
(14) Zhen, G. L.; Falconnet, D.; Kuennemann, E.; Voros, J.; Spencer, N. D.; Textor, M.; Zurcher, S. *Adv. Funct. Mater.* **2006**, *16*, 243−251.
(15) MacDonald, R. C.; MacDonald, R. I.; Menco, B. P. M; Takeshita, K.; Subbarao, N. K.; Hu, L.-R. *Biochim. Biophys. Acta* **1991**, *1061*, 297−303.
(16) Reviakine, I.; Brisson, A. *Langmuir* **2000**, *16*, 1806−1815.
(17) Kurrat, R.; Textor, M.; Ramsden, J. J.; Boni, P.; Spencer, N. D. *Rev. Sci. Instrum.* **1997**, *68*, 2172−2176.
(18) Muller, D. J.; Amrein, M.; Engel, A. *J. Struct. Biol.* **1997**, *119*, 172−188.
(19) Amstad, E.; Zurcher, S.; Mashaghi, A.; Wong, J. Y.; Textor, M.; Reimhult, E. *Small* **2009**, *5*, 1334−1342.
(20) Nishi, M.; Kobayashi, J.; Pechmann, S.; Yamato, M.; Akiyama, Y.; Kikuchi, A.; Uchida, K.; Textor, M.; Yajima, H.; Okano, T. *Biomaterials* **2007**, *28*, 5471−5476.
(21) Broz, P.; Benito, S. M.; Saw, C.; Burger, P.; Heider, H.; Pfisterer, M.; Marsch, S.; Meier, W.; Hunziker, P. *J. Controlled Release* **2005**, *102*, 475−488.
(22) Nardin, C.; Widmer, J.; Winterhalter, M.; Meier, W. *Eur. Phys. J. E* **2001**, *4*, 403−410.
(23) Nardin, C.; Thoeni, S.; Widmer, J.; Winterhalter, M.; Meier, W. *Chem. Commun.* **2000**, *15*, 1433−1434.
(24) Butt, H. J. *Biophys. J.* **1991**, *60*, 777−785.
(25) Marti, A.; Hahner, G.; Spencer, N. D. *Langmuir* **1995**, *11*, 4632−4635.
(26) Muller, D. J.; Engel, A. *Biophys. J.* **1997**, *73*, 1633−1644.
(27) Butt, H. J. *Biophys. J.* **1991**, *60*, 1438−1444.
(28) Pasche, S.; Textor, M.; Meagher, L.; Spencer, N. D.; Griesser, H. J. *Langmuir* **2005**, *21*, 6508−6520.
(29) Kawaguchi, S.; Imai, G.; Suzuki, J.; Miyahara, A.; Kitano, T. *Polymer* **1997**, *38*, 2885−2891.
(30) Ratanabanangkoon, P.; Gropper, M.; Merkel, R.; Sackmann, E.; Gast, A. P. *Langmuir* **2003**, *19*, 1054−1062.
(31) Larsson, C.; Rodahl, M.; Hook, F. *Anal. Chem.* **2003**, *75*, 5080−5087.
(32) Kim, K. T.; Meeuwissen, S. A.; Nolte, R. J. M.; van Hest, J. C. M. *Nanoscale* **2010**, *2*, 844−858.
(33) Menjoge, A. R.; Kannan, R. M.; Tomalia, D. A. *Drug. Discovery Today* **2010**, *15*, 171−185.
(34) Tarahovsky, Y. S. *Biochemistry (Moscow)* **2010**, *75*, 811−824.
(35) Harada, A.; Kataoka, K. *Prog. Polym. Sci.* **2006**, *31*, 949−982.
(36) Graff, A.; Winterhalter, M.; Meier, W. *Langmuir* **2001**, *17*, 919−923.
(37) Boukobza, E.; Sonnenfeld, A.; Haran, G. *J. Phys. Chem. B* **2001**, *105*, 12165−12170.
(38) Kumar, S.; Hoh, J. H. *Langmuir* **2000**, *16*, 9936−9940.
(39) Richter, R.; Mukhopadhyay, A.; Brisson, A. *Biophys. J.* **2003**, *85*, 3035−3047.
(40) Jass, J.; Tjarnhage, T.; Puu, G. *Biophys. J.* **2000**, *79*, 3153−3163.
(41) Vermette, P.; Griesser, H. J.; Kambouris, P.; Meagher, L. *Biomacromolecules* **2004**, *5*, 1496−1502.
(42) Ruozi, B.; Tosi, G.; Forni, F.; Fresta, M.; Vandelli, M. A. *Eur. J. Pharm. Sci.* **2005**, *25*, 81−89.
(43) Stamou, D.; Duschl, C.; Delamarche, E.; Vogel, H. *Angew. Chem., Int. Ed.* **2003**, *42*, 5580−5583.
(44) Vermette, P.; Meagher, L.; Gagnon, E.; Griesser, H. J.; Doillon, C. J. *J. Controlled Release* **2002**, *80*, 179−195.
(45) Degennes, P. G. *Macromolecules* **1980**, *13*, 1069−1075.
(46) Seifert, U.; Lipowsky, R. *Phys. Rev. A* **1990**, *42*, 4768−4771.